JACS
JOURNAL OF THE AMERICAN CHEMICAL SOCIETY

Article

pubs.acs.org/JACS

Structure and Dynamics of the Huntingtin Exon-1 N-Terminus: A Solution NMR Perspective

Maria Baias,[†,#] Pieter E. S. Smith,[†,#,∥] Koning Shen,[‡] Lukasz A. Joachimiak,[‡,⊥] Szymon Żerko,[§] Wiktor Koźmiński,[§] Judith Frydman,[‡] and Lucio Frydman*[,†]

[†]Department of Chemical Physics, Weizmann Institute of Science, Rehovot 76100, Israel

[‡]Stanford University, Stanford, California 94305, United States

[§]Faculty of Chemistry, Biological and Chemical Research Centre, University of Warsaw, Żwirki i Wigury 101, 02-089 Warsaw, Poland

Supporting Information

ABSTRACT: Many neurodegenerative diseases are characterized by misfolding and aggregation of an expanded polyglutamine tract (polyQ). Huntington's Disease, caused by expansion of the polyQ tract in exon 1 of the Huntingtin protein (Htt), is associated with aggregation and neuronal toxicity. Despite recent structural progress in understanding the structures of amyloid fibrils, little is known about the solution states of Htt in general, and about molecular details of their transition from soluble to aggregation-prone conformations in particular. This is an important question, given the increasing realization that toxicity may reside in soluble conformers. This study presents an approach that combines NMR with computational methods to elucidate the structural conformations of Htt Exon 1 in solution. Of particular focus was Htt's N17 domain sited N-terminal to the polyQ tract, which is key to enhancing aggregation and modulate Htt toxicity. Such in-depth structural study of Htt presents a number of unique challenges: the long homopolymeric polyQ tract contains nearly identical residues, exon 1 displays a high degree of conformational flexibility leading to a scaling of the NMR chemical shift dispersion, and a large portion of the backbone amide groups are solvent-exposed leading to fast hydrogen exchange and causing extensive line broadening. To deal with these problems, NMR assignment was achieved on a minimal Htt exon 1, comprising the N17 domain, a polyQ tract of 17 glutamines, and a short hexameric polyProline region that does not contribute to the spectrum. A pH titration method enhanced this polypeptide's solubility and, with the aid of ≤5D NMR, permitted the full assignment of N17 and the entire polyQ tract. Structural predictions were then derived using the experimental chemical shifts of the Htt peptide at low and neutral pH, together with various different computational approaches. All these methods concurred in indicating that low-pH protonation stabilizes a soluble conformation where a helical region of N17 propagates into the polyQ region, while at neutral pH both N17 and the polyQ become largely unstructured—thereby suggesting a mechanism for how N17 regulates Htt aggregation.

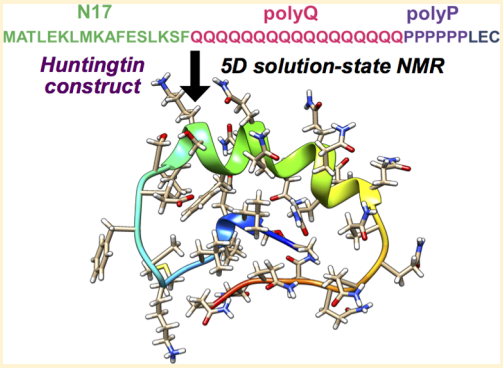

INTRODUCTION

Huntington's Disease (HD) is one of nine known progressive neurodegenerative diseases where expansion of a CAG trinucleotide repeat beyond a threshold length leads to pathogenesis, predominantly through a gain-of-function mechanism.[1] Disease risk and age of onset correlate with length of the polyglutamine (polyQ) tract encoded by the trinucleotide repeat. The aggregation propensity of these disease-linked proteins also correlates with the polyQ repeat length, suggesting that either Q-length dependent aggregation, or some conformation populated along the aggregation pathway, are linked to disease pathology.[2] In fact, studies have suggested that the large amyloid aggregates may be protective, and that toxicity arises from soluble misfolded species, including misfolded versions of the monomer and higher-order oligomers.[3,4] This raises the important question of what are the soluble conformations populated by the polyQ tract in general, and by polyQ in the ∼347 kDa huntington protein (Htt) in particular. Htt is composed of ∼3144 amino acids, and the polymorphic polyQ tract near its N-terminus typically consists between approximately 6 and 35 glutamines.[5−11] A mutation in the Htt gene that extends the polyQ tract beyond 36 residues leads to the development of Huntington's disease.[12] Despite the large size of the protein, the first exon, which contains the polyQ tract (herein Htt-ex1), suffices by itself to induce many of the pathological features of Huntington's disease in cell and animal models.[2] A growing body of evidence suggests that in vivo generation of a fragment containing this exon 1 is necessary for Htt toxicity.[13] The regions flanking the polyQ have been found to modulate Htt aggregation and pathogenicity.[14−18] In particular, Htt-ex1 aggregation is

Received: October 18, 2016
Published: January 13, 2017

DOI: 10.1021/jacs.6b10893
J. Am. Chem. Soc. 2017, 139, 1168−1176

profoundly influenced by the N-domain flanking the polyQ tract:[14,15,19−22] N17, which comprises the first 17 residues of the protein, stimulates aggregate formation of polyQ-expanded Htt both in vitro and in vivo. This domain also influences the interaction of Htt with cellular components, including membranes and chaperones.[14,15,23,24]

The structural impact of N17 on the polyQ tract conformation remains elusive. N17 can form an amphipathic helix, and many studies have suggested that N17 helicity contributes to the aggregation and pathology of Huntington's disease.[25−28] Since Htt has been shown to associate with membranes, the structure of the N17 domain has been explored in micellar mixtures. Here it adopts a helical conformation, with the hydrophobic side chains contained between residues 6 and 17 oriented toward the hydrophobic core of the micelles.[29] This suggests that N17 can behave as a reversible membrane anchor for Htt. Membrane association could create a high local concentration of polyQ at a membrane surface that promotes aggregation.[30] Solid-state NMR studies of an N-terminal Htt fragment resembling the exon 1 segment showed that N17 in amyloid fibrils feature β-sheets at their core, and detected two distinct polyQ folding motifs proximate in space.[31−38] Furthermore, since the N17 domain contains a coiled-coil like sequence, it has been suggested that a helical N17 conformation nucleates aggregation through formation of a 4-helix bundle that brings the polyQ tracts into close proximity.[31−36] However, recent studies have challenged the role of N17's helicity in promoting polyQ aggregation.[25,26,36] Notably, exchanging the N17 domain of Htt for a canonical coiled-coil domain actually suppressed Htt aggregation.[25] These studies suggest that a disordered N17 domain may participate in structural "cross-talk" with a disordered polyQ tract, to promote the amyloid's aggregation. Furthermore, the electrostatics of the regions flanking the polyQ domain may also play an important role in promoting polyQ aggregation. Highly charged sequences flanking the polyQ have been shown to suppress aggregation,[25,26,39] and phosphorylation of serines 13 and 16 in the N17 domain have been shown to impact Huntingtin aggregation and toxicity in vivo and in vitro.[27,28] Thus, understanding the conformational dynamics of the N17 domain is essential to elucidate and eventually control the conversion of Htt to neurotoxic conformations.

The regular structure of amyloid fibrils enables their structural characterization by solid-state NMR, electron microscopy and even crystallography.[15,29−32,37−45] However, many studies have questioned the relevance of fibrillar aggregates to cellular toxicity,[3,4] highlighting the importance of defining the structural properties of soluble Htt conformations. The flexible, structurally heterogeneous and intrinsically disordered nature of soluble Htt exon 1 poses many challenges to structural analyses. The application of high-resolution NMR to Htt's exon 1 fragment in aqueous solution could be highly informative, but is still limited by a lack of ^{15}N and ^{13}C assignments. These assignments could open multiple routes for structural and dynamic investigations, but obtaining them presents several challenges, related to the large number of very similar glutamine residues in the polyQ tract, and to the high degree of mobility observed in the backbone of this fragment.[46−49] A consequence of this high degree of peptide disorder is a fast conformational exchange, which dramatically reduces the chemical shift dispersion and results in extensive spectral overlap. Additionally, as disorder causes the peptide's backbone to be fully solvent exposed, labile amide hydrogens efficiently exchange with the solvent, broadening their spectral NMR lines and further reducing resolution and sensitivity. For peptides that display a high degree of dynamism, these difficulties might be alleviated using a combination of low pH and/or temperature conditions that suppress hydrogen exchange, and partially mitigate the effects of rapid conformational exchange.[50−56]

Using the above strategies and relying on a portfolio of 3D-5D NMR experiments proceeding in combination with nonuniform sampling methods, this work succeeded in assigning backbone ^{13}C and ^{15}N resonances for a 49 residue variant of exon 1 containing the N17 segment, a 17-mer polyQ fragment, a hexaproline tract, and a hexahistidine tag (the "N17Q17" construct; Figure 1). With the aid of variable temperature and pH titration NMR experiments, chemical shift changes were then mapped from low pH to physiological pH conditions, allowing nearly all residues to be identified. These chemical shifts, in combination with numerical calculations, revealed insights into the fragment's structural motifs. At low pH, chemical-shift-based CS-ROSETTA and TALOS+ calculations revealed that the exon 1 fragment possesses significant α-helix propensity in its core region, especially in the transition between the N17 to polyQ region. As the fragment approached physiological pH, however, secondary structure was no longer present: NMR-based CS-ROSETTA and other structural predictors indicate that the peptide collapsed into a disordered conformation—even if encompassing a number of conserved distances. The structural aspects revealed by these data concerning the peptide's solution-phase behavior support the perspective that a disordered N17 domain may promote polyQ aggregation while a highly charged or structured N17 domain may be inhibitory for aggregation. Thus, these results have implications for the development of therapeutics that may stabilize a structured domain for N17 to prevent generation of toxic oligomer or aggregate conformations.

Figure 1. Exon 1 fragment of huntingtin containing the entire N17 domain, a polyQ tract with 17 glutamines, a short polyproline region and an LEC linker before the hexahistidine tag at the C-terminus.

EXPERIMENTAL SECTION

Protein Preparation. The fragment illustrated in Figure 1, henceforth N17Q17, was overexpressed in a Nico *E. coli* BL21 strain. Overnight cultures were diluted 40-fold in Lysogenic broth and growth to an OD of 0.6 at 37 °C. Thereafter, expression was induced with 1 mM IPTG for 4h at 37 °C. Cells were harvested by spinning at 4000*g* for 20 min at 4 °C; pellets were washed with PBS, then respun, flash frozen in LN2, and stored at −80 °C. Pellets were resuspended in Buffer A (50 mM K-Hepes/pH 7.4, 20 mM Imidazole, 8 M urea), sonicated 3x (50% output, 1 s on/off, 1 min), and incubated at room temperature for 30 min. Lysates were cleared by 12 000 rpm spin for 45 min. The supernatant was incubated with Ni-Sepharose beads (GE) for 30 min at room temperature. Protein was purified from the lysate by first washing the beads with Buffer A, then 50 mM K-Hepes/pH 7.4, 20 mM Imidazole with no urea, and finally eluted with 50 mM K-Hepes/pH 7.4, 500 mM Imidazole. Protein was dialyzed against 50 mM Ammonium Formate/pH 3.5 three times for 3 h each. Protein was then lyophilized and stored at −20 °C.

NMR Backbone Resonance Assignments. Backbone resonance assignment experiments were performed on uniformly [^{13}C, ^{15}N] labeled N17Q17 sample dissolved in 10% aqueous formic acid solution

DOI: 10.1021/jacs.6b10893
J. Am. Chem. Soc. 2017, 139, 1168−1176

Table 1. List of Parameters Used for the Assignment of N17Q17 in Vitro at Low pH

		evolution times [ms]						
experiment	total time [h]	N	CO	N	CO	CB	CA	indirect-domains points
HNCO	6.5	100	100					1000
(H)NCO(NCA)CONH	46	40	40	40	40			3175
HNCOCACB	18	40	40			14	10	690

Table 2. List of Parameters Used for the Assignment of N17Q17 in Vitro at Neutral pH

	number of points			spectral width (ppm)				
experiment	F1H	F2N	F3C	F1H	F2N	F3C	no. of scans	recycle delay (ms)
HNCA	768	56	28	3	17	30	8	250
HN(CO)CA	768	56	28	3	17	20	8	250
HN(CA)CO	768	16	28	3	17	8	24	250
HNCO	768	36	28	3	17	60	8	250
HN(CO)CACB	768	56	28	3	17	57	16	100
HNCACB	768	82	28	3	17	30	96	300
HSQC	574	28		3	17		160	300

with 10% D_2O at pH = 1.66 and 25 °C. These experiments were performed on an 800 MHz Agilent DD2 spectrometer equipped with a HCN cold probe. The ^{1}H, ^{13}C and ^{15}N resonances were assigned using 3D HNCO, 5D (H)NCO(NCA)CONH,[57] and 5D HNCO-CACB[57] experiments. In the (H)NCO(NCA)CONH experiment sequential links with N(i)CO(i−1) chemical shifts pair are established. N and CO chemical shifts provide the highest resolution and thus reliability in performing backbone assignment in intrinsically disordered peptides. HNCOCACB allows easy identification of amino acid type. All 5D experiments used sparse random sampling of the indirectly detected time domains,[58] and were processed by multidimensional Fourier transformation using the home written software package (http://nmr.cent3.uw.edu.pl/software). The 3D HNCO spectra were processed using the cleaner3d[59] program to remove sampling artifacts, and later used as base spectra for Sparse Multidimensional Fourier Transform processing of higher dimensionality experiments.[60] Spectra were inspected using Sparky,[61] and their resonance assignment was performed manually. The parameters used for these higher-dimensional experiments are listed in Table 1.

Variable Temperature Experiments. Variable temperature experiments were performed using a Bruker AVANCE III 800 MHz spectrometer on a 110 μM uniformly ^{15}N-labeled N17Q17 sample dissolved in a 50 mM NaPi buffer solution with 10% D_2O, prepared at a pH of 1.75. ^{15}N—^{1}H HSQC spectra were recorded at 25 °C, 20 °C, 15 °C, 10 °C, and 4 °C, with a recycle delay of 300 ms and 96 scans using a data size of 768 (^{1}H) × 36 (^{15}N) points (Table 2). Each experiment was preceded by a 15 min delay to allow for temperature stabilization and shimming was optimized prior to each experiment.

pH Titrations. Titration experiments were performed on the 110 μM uniformly ^{15}N-labeled N17Q17 dissolved in 50 mM NaPi buffer with 10% D_2O and 5 mM DTT at 4 °C, on a Bruker AVANCE III 800 MHz spectrometer. Thirteen different pHs were monitored by adding 10 μL aliquots of 0.2 M aqueous NaOH in 10% D_2O directly into the Shigemi NMR tube. Before and after each aliquot of NaOH was added, a pH value was measured using an SI Analytics microelectrode; the values hence achieved were 1.75, 1.80, 0.197, 2.09, 2.26, 2.52, 2.82, 3.24, 3.87, 4.26, 5.44, 6.55, and 7.08. Each experiment was preceded by a 15 min delay to allow for temperature stabilization at 4 °C. Shimming and pulse calibrations were optimized prior to all experiments; the number of scans acquired varied from 48 to 160, with an increased number of scans were required at higher pH. By comparison with the assigned ^{15}N—^{1}H HSQC spectrum acquired at pH = 7.08, ^{15}N and ^{1}H resonances were identified in a pH = 7.4 dissolved in 50 mM NaPi buffer (with 10% D_2O and 5 mM DTT) acquired at 4 °C. HN, N, C^{α}, C^{β}, and CO chemical shifts were identified in this sample by means of BEST[62] HNCA, HN(CO)CA, HNCACB, HN(CO)CACB, HN(CA)CO, and HNCO experiments. The acquisition parameters for these experiments are given in Table 2. Data were processed with NMRPipe[63] and analyzed using Sparky.[61]

CS-ROSETTA Structure Predictions. Chemical shift derived structures were generated using the CS-ROSETTA[64,65] Web server, on the WeNMR[66] grid. Structure predictions were done for the low and neutral pH conditions, each one of them generating 14000 models.

RESULTS AND DISCUSSION

Backbone Resonance Assignment. The first step in this N17Q17 study included assigning the backbone resonances of the amino acids belonging to the N17 region, and to the 17-glutamine residues of the polyQ. Due to the peptide's conformational flexibility and fast exchange of its labile amide hydrogens with the solvent, the chemical shift dispersion was very limited when such experiments were carried out at physiological pH. This is illustrated by the black contours in Figure 2, which show N17Q17's ^{15}N—^{1}H HSQC spectrum recorded on an aqueous solution at pH = 7.08. Despite the slowing down of the proton amide−solvent exchange rates at the low temperature at which this spectrum was acquired, there is a significant loss of spectral information that prevents establishing the sequential connectivity needed for an NMR

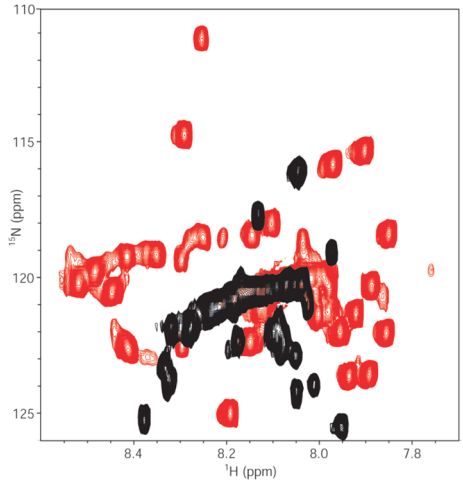

Figure 2. Comparison between the ^{15}N—^{1}H HSQC spectra obtained for N17Q17 in a 10% formic acid solution at 25 °C and pH = 1.66 (red), and in a neutral pH NaPi buffer at 4 °C and pH = 7.08 (black).

DOI: 10.1021/jacs.6b10893
J. Am. Chem. Soc. 2017, 139, 1168−1176

resonance assignment. Direct methods of detection based on ^{13}C and even ^{15}N NMR were also assayed,[67] but also in these instances line broadening was excessive. Only at lower pH was this loss of spectral information substantially mitigated, as can be seen in the ^{15}N—^{1}H HSQC spectrum recorded for N17Q17 in a 10% formic acid solution (red contours in Figure 2). Assignments were therefore obtained for N17Q17 at a pH of 1.7, and the resonances thus identified were mapped to their neutral pH counterparts by acquiring NMR spectra while gradually varying the solution's acidity. Still, conventional 2D and 3D NMR sequences proved incapable of providing an unambiguous peak assignment even at the lowest pH; to implement these assignments, a series of sparsely sampled 3D/5D NMR experiments had to be performed. The 5D experiments focused on two aims: an HNCOCACB served to separate each residue according to a specific spectral signature that revealed its chemical nature; a 5D (H)NCO(NCA)CONH then enabled us to correlate consecutive residues, despite the overlap. With these sequences, the nature of all residues as well as the ensuing chemical shift values of their HN, N, C^{α}, C^{β}, and CO sites in every (nonproline) residue could be elucidated—i.e., a complete "backbone walk" from one end of the polypeptide to the other was feasible (see Figure 3 and

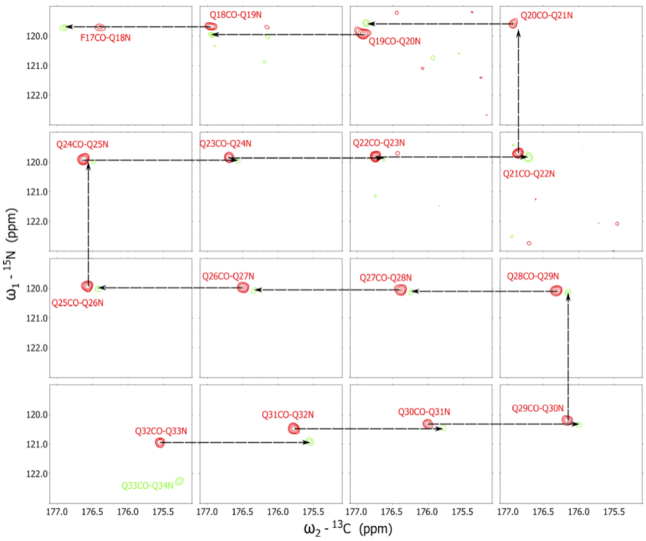

Figure 3. Unambiguous $(NCO)_{i-1} \rightarrow (NCO)_i$ connectivities between consecutive N17Q17 residues arising from 5D (H)NCO(NCA)-CONH NMR at 800 MHz and pH = 1.66. Arrows show correlations observed within the relevant 4D NCO_{i-1} (red contours)−CON_i (green contours) space, for 16 of the polyQs residues (the 17th residue was omitted, and the presentation shown as two-dimensional connectivities to simplify the Figure's graphics).

Experimental Section for details). Figure 4 shows a thus assigned 2D ^{15}N—^{1}H HSQC spectrum of N17Q17 in formic acid; a list of the resonance assignments measured for the C^{α}, C^{β}, and CO sites as well as the shifts for the amides' ^{1}H and ^{15}N, are given in Table S1 of the Supporting Information.

As mentioned, exchange broadening and extreme peak overlapping prevented us from extending this assignment strategy to N17Q17 at physiological pH: neither at low nor room temperatures, could a walk along the peptide's backbone—and therefore a traditional assignment procedure—be performed. In fact at physiological-like conditions, numerous peaks disappeared from the HSQC spectrum, and the data were

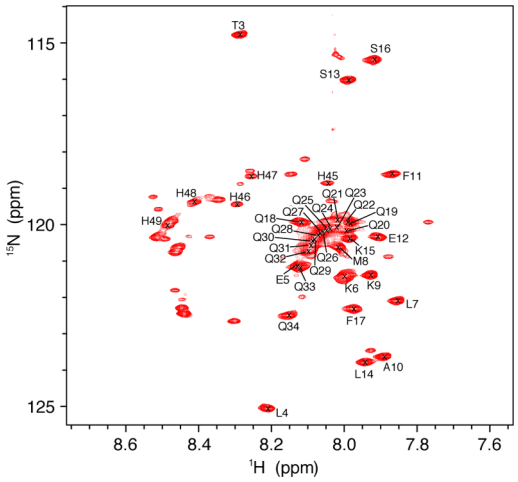

Figure 4. ^{15}N—^{1}H HSQC spectrum of N17Q17 acquired at 25 °C in 10% formic acid (pH = 1.66), showing the assigned backbone amides of all but the first two residues.

of little use. Therefore, a variable temperature and variable pH titration approach was used to correlate the assigned chemical shifts obtained under low pH conditions at 25 °C, to those arising at physiological pH and 4 °C. ^{15}N—^{1}H HSQC spectra were first recorded at pH = 1.7 in order of decreasing temperatures: 25 °C, 20 °C, 15 °C, 10 °C, and 4 °C. The chemical shifts of the resonances assigned at 25 °C could thus be followed, enabling us to assign the majority of the resonances identified in the low pH, 4 °C ^{15}N—^{1}H HSQC spectrum. Figure 5 (left) shows a superposition of spectra acquired at this series of temperatures, highlighting the clear chemical shift trends exhibited by certain residues. By following this trend, a full extrapolation of the high-temperature ^{15}N—^{1}H HSQC assignment could be performed; this is shown in Figure 5 (right).

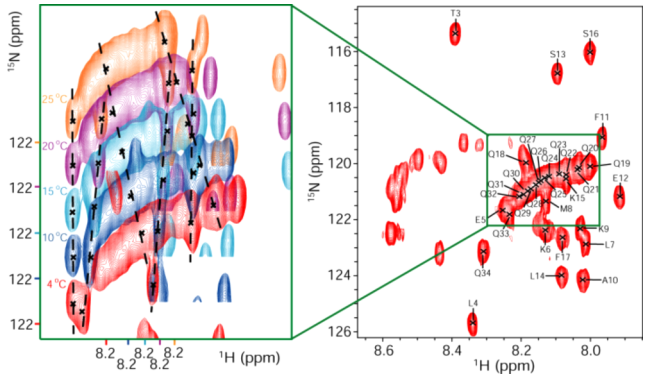

Figure 5. (Left) Superposition of ^{1}H—^{15}N HSQC spectra recorded at different temperatures, following the chemical shift evolution of residues in the green box that is zoomed out in the right-hand panel. Only for the purpose of illustrating these chemical shift changes the variable-temperature spectra in this plot are displayed shifted along both the ^{1}H and ^{15}N dimensions (so as to enable a clearer observation of the trends); the displaced colored ticks along the two axes of the zoomed panel, illustrate the extent of these shifts. The chemical shift range for each spectrum is 7.98 to 8.37 ppm for ^{1}H and 119.7 to 122.3 for ^{15}N. (Right) ^{15}N—^{1}H HSQC spectrum acquired on N17Q17 dissolved in aqueous buffer at pH = 1.75 and T = 4 °C, with assigned backbone amides labeled.

DOI: 10.1021/jacs.6b10893
J. Am. Chem. Soc. 2017, 139, 1168−1176

Following the assignment of the low-temperature, pH = 1.75 structure, NMR titration experiments were repeated at constant temperatures; starting at this low pH and concluding at pH = 7.1. Figure S1 illustrates how this process allowed us to map the assignments in the low pH spectrum to their counterparts at physiological pH. In the spectra shown in that Figure, four resonances were tracked using ^{15}N—^{1}H HSQC spectra recorded at 5 different pH values. The black arrows in Figure S1 highlight resonances whose chemical shifts experience relatively large changes upon increasing sample pH. Using this protocol, a majority of resonances could be identified; an assigned HSQC of N17Q17 at physiological pH is shown in Figure 6. A list of assigned chemical shifts deriving from this

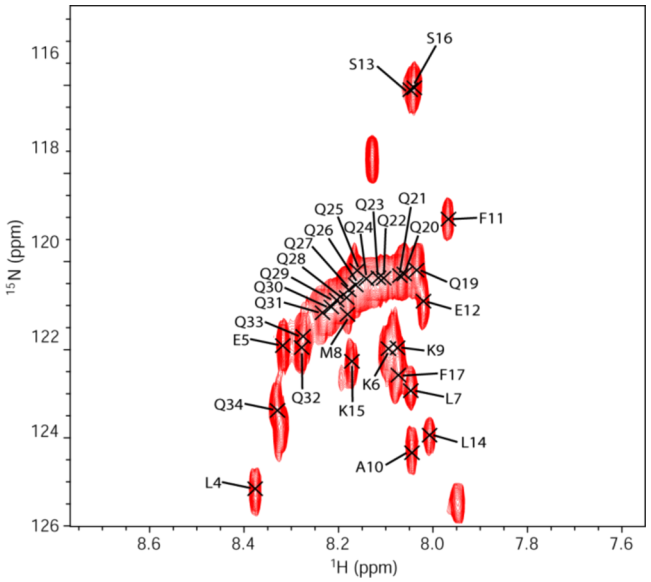

Figure 6. Peak assignments of the ^{15}N—^{1}H HSQC spectrum acquired on N17Q17 dissolved in aqueous buffer at pH = 7.08 and T = 4 °C, with assigned backbone amides labeled according to residue. The Histidine residues disappear with increasing pH; the two unassigned peaks are ascribed to residues from the LEC fragment positioned next to the polyP tract.

assignment and of ancillary HNCO, HNCA, and HNCACB experiments for the backbone and side-chain sites of N17Q17 at neutral pH, is provided in Table S2.

NMR-Derived Structural Information. The availability of ^{1}H, ^{15}N, and ^{13}C chemical shifts for various residues enables one to estimate the fractional populations of secondary structural elements in N17Q17. This analysis was initially accomplished using the Secondary Structure Propensity (SSP) program[68] with the ^{13}C chemical shift values identified for the C$^{\alpha}$ and C$^{\beta}$ sites of the various residues as inputs, as it has been demonstrated before that these chemical shifts are more relevant for predicting secondary structure propensities of intrinsically disordered proteins.[68] As a reminder, in folded proteins consecutive residues with SSP values of +1 indicate α-helical structure, and consecutive residues with SSP values of −1 indicate a β-strand. Consecutive residues with positive or negative SSP values reveal a disordered protein, with the weighted average of the local fractional populations being the secondary structures (α-helix or β-strand) exhibited by the ensemble of conformers. Figure 7a shows SSP scores for the assigned residues of N17Q17; in black for the low pH and in red for the neutral pH structure. At low pH, the N17Q17

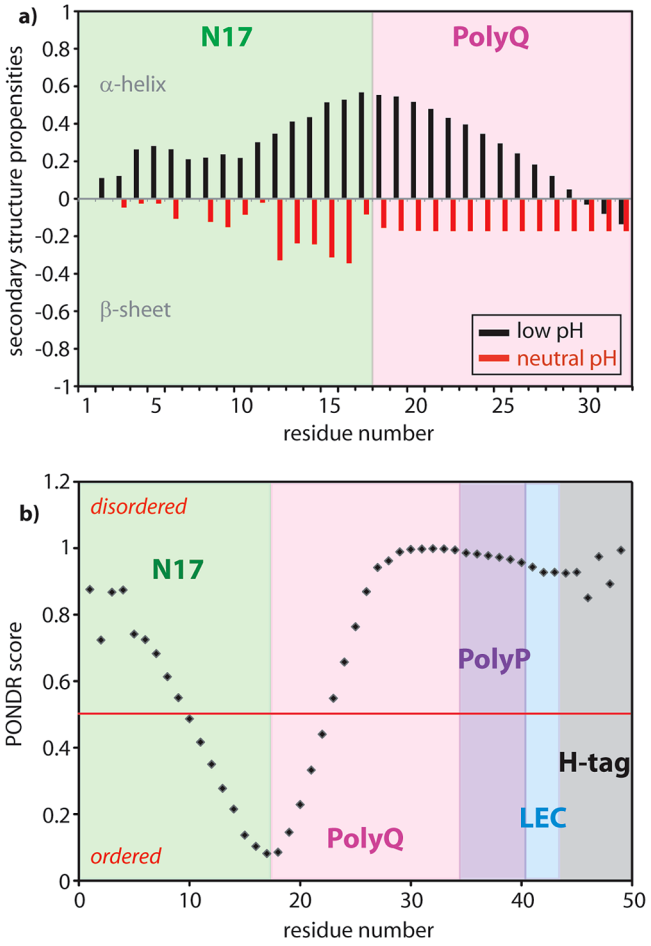

Figure 7. (a) Secondary structure propensity (SSP) values[68] derived for the N17Q17 backbone in 10% aqueous formic acid solution (pH = 1.66; 25 °C; black) and in NaPi buffer (pH = 7.4; 4 °C; red). SSPs were calculated using C$^{\alpha}$ and C$^{\beta}$ chemical shifts. (b) Dynamic disorder analysis of the N17Q17 peptide, performed using the amino acid sequence as input and using the VX-LT predictor of PONDR.[69,70]

ensemble of conformers exhibits a clear propensity for α-helical structures forming in the central region of the peptide. This trend changes as pH increases, culminating with a structurally disordered structure—even one exhibiting slight β-sheet propensity—at physiological pH. To complement these shift-based propensity analyses, the naturally disordered regions in N17Q17 were explored using the PONDR[72,73] algorithm. A PONDR score above 0.5 indicates disorder, while a score below 0.5 indicates order in the protein. Out of the 49 residues in N17Q17, 36 were found to be disordered, constituting ∼75% of the peptide's backbone (Figure 7b). A higher degree of order is predicted for residues 10−22 (AFESLKSFQQQQQ) at the junction of the N17 headpiece and the polyQ domain.

Such strong pH effects on the conformation and degree of order in a protein have been interpreted in terms of electrostatics.[71−76] For Htt exon 1, electrostatics have been shown to modulate the effect of the N17 domain on the proximal polyQ tract, as exchanging N17 for a highly charged lysine-containing domain in an Htt chimera construct inhibited polyQ aggregation.[26] Indeed, the introduction of negative charge via phosphorylation of Serines 13 and 16 (or via Ser-to-Asp mutations) in N17, reduces Htt aggregation propensity, changes aggregate morphology, and importantly, abrogates disease symptoms in a mouse model of Huntington's disease.[27]

DOI: 10.1021/jacs.6b10893
J. Am. Chem. Soc. 2017, 139, 1168−1176

Our analyses find that at low pH, N17 tends to adopt a α-helix. Interestingly, N17Q17 is also much more soluble at low pH than at neutral pH (Figure S2). This suggests a correlation between N17Q17's low pH structure and the higher solubility brought about by this Htt conformation. These results align with recent reports according to which the electrostatics of regions flanking the polyQ domain heavily influence domain cross-talk and the readiness of the polyQ to adopt an aggregation-prone, molten globule state.[25,26,77] One could expect that at low pH, the highly charged flanking sequences will be less likely to engage in aggregation-prone "cross-talk" between the polyQ domain and flanking sequences, thus disfavoring the formation of a molten globule collapsed state.[25,77] Upon raising the pH, the overall charge of the entire peptide, including that of the N17 fragment, will decrease; this induces disorder in both the N17 and polyQ regions, leading to an enhanced domain cross-talk between the N17 and polyQ regions and promoting the generation of conformers that lead to amyloid aggregation. Further investigations are necessary and in progress, to fully understand and ascertain this role of electrostatics in modulating the soluble Htt exon 1 fragment's behavior.

To deepen our structural understanding of these low and neutral pH states of Htt, we compared the SSP and PONDR results with models arising from CS-ROSETTA calculations—a methodology that although based on homology modeling of folded protein structures, has also been successfully applied to understand disordered protein fragments.[78,79] To this end, the ^{13}CO, $^{13}C\alpha$, and $^{13}C\beta$ chemical shifts extracted from 3D BEST NMR experiments at low and neutral pH were fed into CS-ROSETTA; Figure 8 shows the lowest score structures that emerge from this program. As had been observed using SSP and PONDR, this approach also reveals a low pH α-helical structure in the core region of the peptide, between residues Leu14 and Gln26 (Figure 8a). Also in agreement with the SSP and PONDR calculations, CS-ROSETTA shows that N17 helicity is lost when moving to neutral pH, where two separate sets of CS-ROSETTA simulations reveal disordered, coiled conformations for the entire peptide (Figure 8b). Interestingly, however, these two conformations are not entirely random: different regions of the peptide remain connected via hydrogen bonds, that according to these calculations still endow the peptide with a globular shape at neutral pH. It remains to be seen whether this is a result of Rosetta attempting to satisfy hydrogen bond donors/acceptors, or a genuine molten globule structure.

The peptide's backbone dynamics was also probed via molecular dynamics simulations, using as starting point the lowest score CS-ROSETTA structures. 100 ns trajectories were simulated for both the low pH and the neutral pH structures. As can be appreciated in Figure S3, at low pH the backbone of the peptide shows a more rigid central region where the formation of a α-helical secondary structure can be recognized. This is in agreement with the CS-ROSETTA, PONDR, and SSP results. By contrast, at near physiological pH and low temperature (Figure S4) MD indicates—also in agreement with the other computations—that backbone secondary structure is no longer present—even if the peptide does not depart from a globular character. It remains to be seen whether this globular nature would persist at longer-time trajectories. Therefore, another corroboration of this insight on the backbone peptide dynamics was sought by a TALOS-based chemical shift-based secondary structure analyses;[80] this

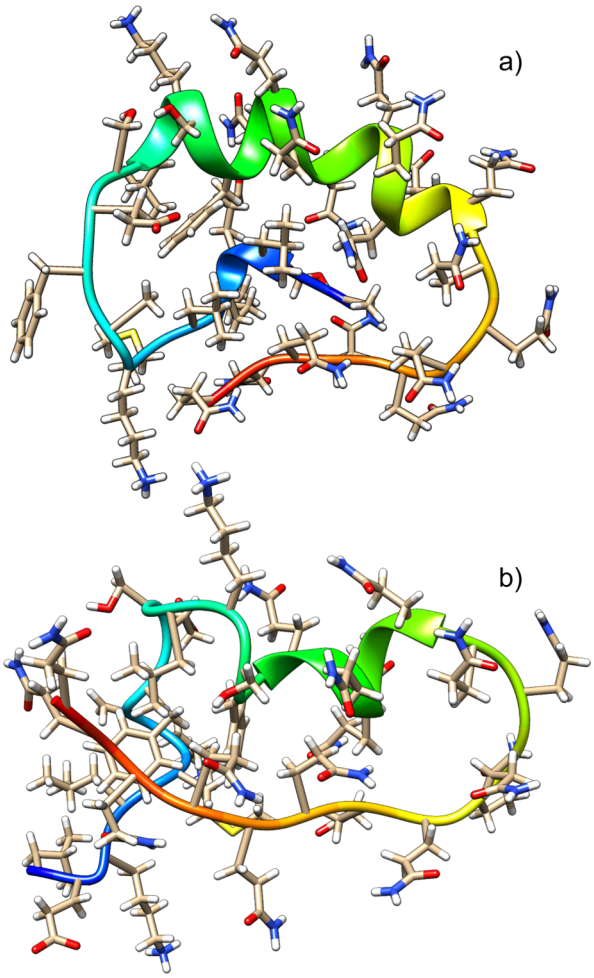

Figure 8. Lowest score CS-ROSETTA structures predicted from the NMR data at (a) low pH and (b) neutral pH. Whereas the low pH structure exhibits a clear α-helical core, at neutral pH all secondary structure disappears. The structure, however, does not collapse into an entirely random coil: hydrogen bonds between residues Lys15 and Gln18 (1.9 Å), Ser16 and Gln28 (2.8 Å), Gln19 and Gln23 (1.98 Å), and Gln20 and Gln29 (1.9 Å), remain even at neutral pH.

corroborated the general picture provided by all other computational approaches, showing that a helical stretch extending from Lys15 to Gln25 at low pH, is substantially lost at neutral pH (Figure S5). Finally, a variety of relaxation and Overhauser enhancement measurements were performed to assess how these structural changes affect the backbone's dynamics, but these proved too ambiguous due to the severe peak overlap observed in 3D NMR experiments that incorporated relaxation weightings (data not shown).

CONCLUSIONS

Obtaining structural information on Htt and other polyQ tract proteins in solution is necessary to understand their conversion to pathogenic conformations. NMR measurements were here combined with computations to obtain structural insights into the dynamic soluble conformation of Huntingtin's N-terminal fragment. Thanks to a suite of high-dimensional 800 MHz NMR experiments, ^{1}H, ^{13}C, and ^{15}N backbone and side chain resonances could be successfully assigned for most residues in a 49mer fragment of Huntingtin's N-terminal exon 1 region at acidic pH. Variable temperature and pH titration experiments

DOI: 10.1021/jacs.6b10893
J. Am. Chem. Soc. 2017, 139, 1168−1176

mapped these assignments onto physiological pH conditions, allowing us to identify many residue resonances at neutral pH despite the worsening resolution. An interesting feature revealed by these assignments is the monotonous change of the backbone ^{13}C chemical shifts along the polyQ tract (Tables S1 and S2); given the considerable disorder that characterizes this segment, this could reflect electrostatic differences between the two edges of the homopolymer. The ensuing chemical shift information was used, in combination with SSP, PONDR, CS-ROSETTA, TALOS+, and MD calculations, to extract insight on the solution conformation of the N17Q17 structure. Despite their different database trainings these multiple approaches coincided in concluding that at low pH, the central region of N17Q17 adopts a α-helical secondary structure characterized by reduced internal backbone mobility. Calculations also agreed that helicity disappears at neutral pH, leading to an enhanced disorder. This change in conformation between low and neutral pH likely derives from the influence of electrostatics on the Htt structure. These factors are also likely involved in N17Q17's different aggregation behavior as a function of pH/structure. While this fragment is very soluble at low pH, when it is charged and helical, it becomes more disordered and aggregation prone at neutral pH. This suggests that loss of N17's ordered nature leads to enhanced aggregation, perhaps by promoting the availability of N17 to structurally cross-talk with the polyQ chain (e.g., Figures 8b and S4) and with similar residues in other peptides. This enhanced ability of a disordered N17 fragment to probe an ensemble of aggregation conformations, may also facilitate Htt's amyloidogenic propensities. This could also explain why chaperones or ligands that bind and stabilize N17, such as chaperonins and Htt intrabodies, prevent Htt aggregation.[15,81] If further confirmed, then these structural perspectives might shed new light into the factors promoting amyloidogenic conformations, and open possible therapeutic avenues.

Our results resonate with a recent study that investigated the effect of a tetraleucine (LLLL) segment N-terminally flanking the polyQ25 tract of the androgen receptor (AR), which is linked to another polyQ expansion neurodegenerative disorder called Kennedy's disease.[82] In this case, the flanking LLLL increased the helical propensity of the polyQ and, consistent with our conclusions, decreased its aggregation propensity. It is striking that observations for two different polyQ-expanded, disease-linked proteins, Huntingtin, and AR indicate that an increased helical propensity in the polyQ decreases its proclivity to aggregation. Furthermore, both studies show that sequences flanking the polyQ influence its aggregating nature by modulating its secondary structure. This points to a shared structural principle linking polyQ dynamics and formation of toxic aggregates, and highlights the potential of therapeutics that target these flanking sequences to stabilize polyQ helicity.[15,81]

■ ASSOCIATED CONTENT

Supporting Information

The Supporting Information is available free of charge on the ACS Publications website at DOI: 10.1021/jacs.6b10893.

Figures and Tables containing: Selected ^{1}H—^{15}N HSQC spectra at variable pH titration experiments, T = 4 °C; N17Q17 solubility measurements at different pH; contact maps for different N17Q17 residues at neutral pH; MD 100 ns trajectories at low and neutral pH with representative structures; ^{1}H, ^{15}N, ^{13}CO, $^{13}C\alpha$, and $^{13}C\beta$ assignments and chemical shift values for the various N17Q17 residues at low and neutral pH; and outcome of TALOS calculations (PDF)

■ AUTHOR INFORMATION

Corresponding Author

*lucio.frydman@weizmann.ac.il

ORCID

Lucio Frydman: 0000-0001-8208-3521

Present Addresses

[‖]Florida State University/National High Magnetic Field Laboratory, United States

[⊥]UTSW, United States

[¶]NYU-Abu Dhabi, United Arab Emirates

Author Contributions

[#]These authors contributed equally.

Funding

This research was funded by the Israel Science Foundation grant 795/13, by the I-CORE Program for the Planning and Budgeting Committee (ISF grant 1775/12), by the FP7 BioNMR project (grant contract 261863), by the NIH grants 2PN2EY016525 and NS092525 (to J.F.), and by the generosity of the Perlman Family Foundation. P.E.S.S. is grateful for support from the National Institute on Aging (NIH) in the form of a National Research Service Award fellowship (1F32AG040957-01A1). K.S. was supported by an NSF Graduate Fellowship and a Stanford Graduate Fellowship.

Notes

The authors declare no competing financial interest.

■ ACKNOWLEDGMENTS

We thank Drs. Martin S. Nausner and Tali Scherf for help in setting up NMR experiments and Prof. Tatyana Polenova for useful discussions. The WeNMR project (European FP7 e-Infrastructure grant, contract no. 261572, www.wenmr.eu) and the European Regional Development Fund under the Operational Program Innovative Economy, are also acknowledged.

■ REFERENCES

(1) Ross, C. A. *Neuron* **2002**, *35*, 819.

(2) Bates, G. P.; Benn, C. In *Huntington's Disease*; Oxford University Press: Oxford, 2002; p 429.

(3) Nucifora, L. G.; Burke, K. A.; Feng, X.; Arbez, N.; Zhu, S.; Miller, J.; Yang, G.; Ratovitski, T.; Delannoy, M.; Muchowski, P. J.; Finkbeiner, S.; Legleiter, J.; Ross, C. A.; Poirier, M. A. *J. Biol. Chem.* **2012**, *287*, 16017.

(4) Arrasate, M.; Mitra, S.; Schweitzer, E. S.; Segal, M. R.; Finkbeiner, S. *Nature* **2004**, *431*, 805.

(5) Zuccato, C.; Valenza, M.; Cattaneo, E. *Physiol. Rev.* **2010**, *90*, 905.

(6) Costa, M. d. C.; Magalhaes, P.; Guimaraes, L.; Maciel, P.; Sequeiros, J.; Sousa, A. *J. Hum. Genet.* **2006**, *51*, 189.

(7) Hećimović, S.; Klepac, N.; Vlašić, J.; Vojta, A.; Janko, D.; Škarpa-Prpić, I.; Canki-Klain, N.; Marković, D.; Božikov, J.; Relja, M.; Pavelić, K. *Hum. Mutat.* **2002**, *20*, 233.

(8) Wang, C. K.; Wu, Y. R.; Hwu, W. L.; Chen, C. M.; Ro, L. S.; Chen, S. T.; Gwinn-Hardy, K.; Yang, C. C.; Wu, R. M.; Chen, T. F.; Wang, H. C.; Chao, M. C.; Chiu, M. J.; Lu, C. J.; Lee-Chen, G. J. *Eur. Neurol.* **2004**, *52*, 96.

(9) Nakashima, K.; Watanabe, Y.; Kusumi, M.; Nanba, E.; Maeoka, Y.; Nakagawa, M.; Igo, M.; Irie, H.; Ishino, H.; Fujimoto, A.; Goto, J.; Takahashi, K. *Neuroepidemiology* **2004**, *15*, 126.

DOI: 10.1021/jacs.6b10893
J. Am. Chem. Soc. 2017, 139, 1168−1176

(10) Pramanik, S.; Basu, P.; Gangopadhaya, P. K.; Sinha, K. K.; Jha, D. K.; Sinha, S.; Das, S. K.; Maity, B. K.; Mukherjee, S. C.; Roychoudhuri, S.; Majumder, P. P. *Eur. J. Hum. Genet.* **2000**, *8*, 678.
(11) Morovvati, S.; Nakagawa, M.; Osame, M.; Karami, A. *Arch. Med. Res.* **2008**, *39*, 131.
(12) Andresen, J. M.; Gayán, J.; Djoussé, L.; Roberts, S.; Brocklebank, D.; Cherny, S. S.; The, U. S. V. C. R. G.; The, H. D. M. C. R. G.; Cardon, L. R.; Gusella, J. F.; MacDonald, M. E.; Myers, R. H.; Housman, D. E.; Wexler, N. S. *Ann. Hum. Genet.* **2007**, *71*, 295.
(13) Graham, R. K.; Deng, Y.; Slow, E. J.; Haigh, B.; Bissada, N.; Lu, G.; Pearson, J.; Shehadeh, J.; Bertram, L.; Murphy, Z.; Warby, S. C.; Doty, C. N.; Roy, S.; Wellington, C. L.; Leavitt, B. R.; Raymond, L. A.; Nicholson, D. W.; Hayden, M. R. *Cell* **2006**, *125*, 1179.
(14) Thakur, A. K.; Jayaraman, M.; Mishra, R.; Thakur, M.; Chellgren, V. M.; L Byeon, I.-J.; Anjum, D. H.; Kodali, R.; Creamer, T. P.; Conway, J. F.; M Gronenborn, A.; Wetzel, R. *Nat. Struct. Mol. Biol.* **2009**, *16*, 380.
(15) Tam, S.; Spiess, C.; Auyeung, W.; Joachimiak, L.; Chen, B.; Poirier, M. A.; Frydman, J. *Nat. Struct. Mol. Biol.* **2009**, *16*, 1279.
(16) Gu, X.; Greiner, E. R.; Mishra, R.; Kodali, R.; Osmand, A.; Finkbeiner, S.; Steffan, J. S.; Thompson, L. M.; Wetzel, R.; Yang, X. W. *Neuron* **2009**, *64*, 828.
(17) Crick, S. L.; Ruff, K. M.; Garai, K.; Frieden, C.; Pappu, R. V. *Proc. Natl. Acad. Sci. U. S. A.* **2013**, *110*, 20075.
(18) Caron, N. S.; Desmond, C. R.; Xia, J.; Truant, R. *Proc. Natl. Acad. Sci. U. S. A.* **2013**, *110*, 14610.
(19) Kim, M. W.; Chelliah, Y.; Kim, S. W.; Otwinowski, Z.; Bezprozvanny, I. *Structure* **2009**, *17*, 1205.
(20) Pieri, L.; Madiona, K.; Bousset, L.; Melki, R. *Biophys. J.* **2012**, *102*, 2894.
(21) Sahl, S. J.; Weiss, L. E.; Duim, W. C.; Frydman, J.; Moerner, W. *Sci. Rep.* **2012**, *2*, 895.
(22) Borwankar, T.; Röthlein, C.; Zhang, G.; Techen, A.; Dosche, C.; Ignatova, Z. *Biochemistry* **2011**, *50*, 2048.
(23) Rockabrand, E.; Slepko, N.; Pantalone, A.; Nukala, V. N.; Kazantsev, A.; Marsh, J. L.; Sullivan, P. G.; Steffan, J. S.; Sensi, S. L.; Thompson, L. M. *Hum. Mol. Genet.* **2006**, *16*, 61.
(24) Atwal, R. S.; Xia, J.; Pinchev, D.; Taylor, J.; Epand, R. M.; Truant, R. *Hum. Mol. Genet.* **2007**, *16*, 2600.
(25) Kokona, B.; Rosenthal, Z. P.; Fairman, R. *Biochemistry* **2014**, *53*, 6738.
(26) Kokona, B.; Johnson, K. A.; Fairman, R. *Biochemistry* **2014**, *53*, 6747.
(27) Gu, X.; Greiner, E. R.; Mishra, R.; Kodali, R.; Osmand, A.; Finkbeiner, S.; Steffan, J. S.; Thompson, L. M.; Wetzel, R.; Yang, X. W. *Neuron* **2009**, *64*, 828.
(28) Atwal, R. S.; Desmond, C. R.; Caron, N.; Maiuri, T.; Xia, J.; Sipione, S.; Truant, R. *Nat. Chem. Biol.* **2011**, *7*, 453.
(29) Michalek, M.; Salnikov; Evgeniy, S.; Bechinger, B. *Biophys. J.* **2013**, *105*, 699.
(30) Michalek, M.; Salnikov, E. S.; Werten, S.; Bechinger, B. *Biochemistry* **2013**, *52*, 847.
(31) Sivanandam, V. N.; Jayaraman, M.; Hoop, C. L.; Kodali, R.; Wetzel, R.; van der Wel, P. C. A. *J. Am. Chem. Soc.* **2011**, *133*, 4558.
(32) Mishra, R.; Hoop, C. L.; Kodali, R.; Sahoo, B.; van der Wel, P. C. A.; Wetzel, R. *J. Mol. Biol.* **2012**, *424*, 1.
(33) Mishra, R.; Jayaraman, M.; Roland, B. P.; Landrum, E.; Fullam, T.; Kodali, R.; Thakur, A. K.; Arduini, I.; Wetzel, R. *J. Mol. Biol.* **2012**, *415*, 900.
(34) Jayaraman, M.; Kodali, R.; Sahoo, B.; Thakur, A. K.; Mayasundari, A.; Mishra, R.; Peterson, C. B.; Wetzel, R. *J. Mol. Biol.* **2012**, *415*, 881.
(35) Wetzel, R. in *Protein Misfolding Diseases*; John Wiley & Sons, Inc.: Hoboken, NJ, 2010; p 305.
(36) Fiumara, F.; Fioriti, L.; Kandel, E. R.; Hendrickson, W. A. *Cell* **2010**, *143*, 1121.
(37) Isas, J. M.; Langen, R.; Siemer, A. B. *Biochemistry* **2015**, *54*, 3942.
(38) Hoop, C. L.; Lin, H. K.; Kar, K.; Magyarfalvi, G.; Lamley, J. M.; Boatz, J. C.; Mandal, A.; Lewandowski, J. R.; Wetzel, R.; Van Der Wel, P. C. *Proc. Natl. Acad. Sci. U. S. A.* **2016**, *113*, 1546.
(39) Bhattacharyya, A.; Thakur, A. K.; Chellgren, V. M.; Thiagarajan, G.; Williams, A. D.; Chellgren, B. W.; Creamer, T. P.; Wetzel, R. *J. Mol. Biol.* **2006**, *355*, 524.
(40) Lakhani, V. V.; Ding, F.; Dokholyan, N. V. *PLoS Comput. Biol.* **2010**, *6*, e1000772.
(41) Zhang, Q. C.; Yeh, T.-l.; Leyva, A.; Frank, L. G.; Miller, J.; Kim, Y. E.; Langen, R.; Finkbeiner, S.; Amzel, M. L.; Ross, C. A.; Poirier, M. A. *J. Biol. Chem.* **2011**, *286*, 8188.
(42) Legleiter, J.; Lotz, G. P.; Miller, J.; Ko, J.; Ng, C.; Williams, G. L.; Finkbeiner, S.; Patterson, P. H.; Muchowski, P. J. *J. Biol. Chem.* **2009**, *284*, 21647.
(43) Nagai, Y.; Inui, T.; Popiel, H. A.; Fujikake, N.; Hasegawa, K.; Urade, Y.; Goto, Y.; Naiki, H.; Toda, T. *Nat. Struct. Mol. Biol.* **2007**, *14*, 332.
(44) Wälti, M. A.; Ravotti, F.; Arai, H.; Glabe, C. G.; Wall, J. S.; Böckmann, A.; Riek, R. *Proc. Natl. Acad. Sci. U. S. A.* **2016**, *113*, E4976.
(45) Tuttle, M. D.; Comellas, G.; Nieuwkoop, A. J.; Covell, D. J.; Berthold, D. A.; Kloepper, K. D.; Rienstra, C. M. *Nat. Struct. Mol. Biol.* **2016**, *23*, 409.
(46) Hsu, S.-T. D.; Bertoncini, C. W.; Dobson, C. M. *J. Am. Chem. Soc.* **2009**, *131*, 7222.
(47) Eliezer, D. *Curr. Opin. Struct. Biol.* **2009**, *19*, 23.
(48) Dunker, A. K.; Silman, I.; Uversky, V. N.; Sussman, J. L. *Curr. Opin. Struct. Biol.* **2008**, *18*, 756.
(49) Dyson, H. J.; Wright, P. E. *Nat. Rev. Mol. Cell Biol.* **2005**, *6*, 197.
(50) van Mierlo, C. P. M.; Darby, N. J.; Keeler, J.; Neuhaus, D.; Creighton, T. E. *J. Mol. Biol.* **1993**, *229*, 1125.
(51) Fiebig, K. M.; Rice, L. M.; Pollock, E.; Brunger, A. T. *Nat. Struct. Biol.* **1999**, *6*, 117.
(52) Sigalov, A. B.; Kim, W. M.; Saline, M.; Stern, L. J. *Biochemistry* **2008**, *47*, 12942.
(53) Jaravine, V. A.; Zhuravleva, A. V.; Permi, P.; Ibraghimov, I.; Orekhov, V. Y. *J. Am. Chem. Soc.* **2008**, *130*, 3927.
(54) Noda, Y.; Yokota, A.; Horii, D.; Tominaga, T.; Tanisaka, Y.; Tachibana, H.; Segawa, S.-i. *Biochemistry* **2002**, *41*, 2130.
(55) Delak, K.; Harcup, C.; Lakshminarayanan, R.; Sun, Z.; Fan, Y.; Moradian-Oldak, J.; Evans, J. S. *Biochemistry* **2009**, *48*, 2272.
(56) Buchko, G.; Bekhazi, J.; Cort, J.; Valentine, N.; Snead, M.; Shaw, W. *Biomol. NMR Assignments* **2008**, *2*, 89.
(57) Zawadzka-Kazimierczuk, A.; Koźmiński, W.; Šanderová, H.; Krásný, L. *J. Biomol. NMR* **2012**, *52*, 329.
(58) Kazimierczuk, K.; Zawadzka, A.; Koźmiński, W.; Zhukov, I. *J. Biomol. NMR* **2006**, *36*, 157.
(59) Stanek, J.; Koźmiński, W. *J. Biomol. NMR* **2010**, *47*, 65.
(60) Kazimierczuk, K.; Zawadzka-Kazimierczuk, A.; Koźmiński, W. *J. Magn. Reson.* **2010**, *205*, 286.
(61) Goddard, T. D.; Kneller, D. G. *SPARKY 3*; University of California, San Francisco, 2008.
(62) Lescop, E.; Schanda, P.; Brutscher, B. *J. Magn. Reson.* **2007**, *187*, 163.
(63) Delaglio, F.; Grzesiek, S.; Vuister, G.; Zhu, G.; Pfeifer, J.; Bax, A. *J. Biomol. NMR* **1995**, *6*, 277.
(64) Shen, Y.; Lange, O.; Delaglio, F.; Rossi, P.; Aramini, J. M.; Liu, G.; Eletsky, A.; Wu, Y.; Singarapu, K. K.; Lemak, A.; Ignatchenko, A.; Arrowsmith, C. H.; Szyperski, T.; Montelione, G. T.; Baker, D.; Bax, A. *Proc. Natl. Acad. Sci. U. S. A.* **2008**, *105*, 4685.
(65) Shen, Y.; Vernon, R.; Baker, D.; Bax, A. *J. Biomol. NMR* **2009**, *43*, 63.
(66) Wassenaar, T.; van Dijk, M.; Loureiro-Ferreira, N.; van der Schot, G.; de Vries, S.; Schmitz, C.; van der Zwan, J.; Boelens, R.; Giachetti, A.; Ferella, L.; Rosato, A.; Bertini, I.; Herrmann, T.; Jonker, H. A.; Bagaria, A.; Jaravine, V.; Güntert, P.; Schwalbe, H.; Vranken, W.; Doreleijers, J.; Vriend, G.; Vuister, G.; Franke, D.; Kikhney, A.; Svergun, D.; Fogh, R.; Ionides, J.; Laue, E.; Spronk, C.; Jurkša, S.; Verlato, M.; Badoer, S.; Dal Pra, S.; Mazzucato, M.; Frizziero, E.; Bonvin, A. J. J. *J. Grid Computing* **2012**, *10*, 743.

DOI: 10.1021/jacs.6b10893
J. Am. Chem. Soc. 2017, 139, 1168−1176

(67) Bermel, W.; Felli, I. C.; Kümmerle, R.; Pierattelli, R. *Concepts Magn. Reson., Part A* **2008**, *32A*, 183.
(68) Marsh, J. A.; Singh, V. K.; Jia, Z.; Forman-Kay, J. D. *Protein Sci.* **2006**, *15*, 2795.
(69) Romero, P.; Obradovic, Z.; Dunker, A. K. *Genome Informatics* **1997**, *8*, 110.
(70) Romero, P.; Obradovic, Z.; Li, X.; Garner, E. C.; Brown, C. J.; Dunker, A. K. *Proteins: Struct., Funct., Genet.* **2001**, *42*, 38.
(71) Nielsen, J. E. In *Ann. Rep. Comp. Chem.*; Ralph, A. W., David, C. S., Eds.; Elsevier: 2008; Vol. *4*, p 89.
(72) Lindman, S.; Linse, S.; Mulder, F. A. A.; André, I. *Biochemistry* **2006**, *45*, 13993.
(73) Schubert, M.; Poon, D. K. Y.; Wicki, J.; Tarling, C. A.; Kwan, E. M.; Nielsen, J. E.; Withers, S. G.; McIntosh, L. P. *Biochemistry* **2007**, *46*, 7383.
(74) Fitch, C. A.; Karp, D. A.; Lee, K. K.; Stites, W. E.; Lattman, E. E.; García-Moreno, E. B. *Biophys. J.* **2002**, *82*, 3289.
(75) Schwehm, J. M.; Fitch, C. A.; Dang, B. N.; García-Moreno, E. B.; Stites, W. E. *Biochemistry* **2003**, *42*, 1118.
(76) Lindman, S.; Linse, S.; Mulder, F. A. A.; André, I. *Biophys. J.* **2007**, *92*, 257.
(77) Williamson, T. E.; Vitalis, A.; Crick, S. L.; Pappu, R. V. *J. Mol. Biol.* **2010**, *396*, 1295.
(78) Wang, R.Y.-R.; Han, Y.; Krassovsky, K.; Sheffler, W.; Tyka, M.; Baker, D. *PLoS One* **2011**, *6*, e22060.
(79) Szymczyna, B. R.; Taurog, R. E.; Young, M. J.; Snyder, J. C.; Johnson, J. E.; Williamson, J. R. *Structure* **2009**, *17*, 499.
(80) Shen, Y.; Delaglio, F.; Cornilescu, G.; Bax, A. *J. Biomol. NMR* **2009**, *44*, 213.
(81) Schiefner, A.; Chatwell, L.; Korner, J.; Neumaier, I.; Colby, D. W.; Volkmer, R.; Wittrup, K. D.; Skerra, A. *J. Mol. Biol.* **2011**, *414*, 337.
(82) Eftekharzadeh, B.; Piai, A.; Chiesa, G.; Mungianu, D.; García, J.; Pierattelli, R.; Felli, I. C.; Salvatella, X. *Biophys. J.* **2016**, *110*, 2361.

DOI: 10.1021/jacs.6b10893
J. Am. Chem. Soc. 2017, 139, 1168−1176